MATEUSZ JĘDRZEJEWSKI[1]*, MARTA POĆWIERZ*[1]*, KATARZYNA ZIELONKO-JUNG*[2]

THE PROBLEM OF AIRFLOW AROUND BUILDING CLUSTERS IN DIFFERENT CONFIGURATIONS

In the paper, the authors discuss the construction of a model of an exemplary urban layout. Numerical simulation has been performed by means of a commercial software Fluent using two different turbulence models: the popular k-ε realizable one, and the Reynolds Stress Model (RSM), which is still being developed. The former is a 2-equations model, while the latter – is a RSM model – that consists of 7 equations. The studies have shown that, in this specific case, a more complex model of turbulence is not necessary. The results obtained with this model are not more accurate than the ones obtained using the RKE model. The model, scale 1:400, was tested in a wind tunnel. The pressure measurement near buildings, oil visualization and scour technique were undertaken and described accordingly. Measurements gave the quantitative and qualitative information describing the nature of the flow. Finally, the data were compared with the results of the experiments performed. The pressure coefficients resulting from the experiment were compared with the coefficients obtained from the numerical simulation. At the same time velocity maps and streamlines obtained from the calculations were combined with the results of the oil visualisation and scour technique.

1. Introduction

Wind engineering is a relatively young scientific discipline, dating back to the 1930s. The discipline combines multiple areas of science, including fluid mechanics, construction, architecture and strength of structures. This field of study has been developing for the last 50 years.

[1]*Warsaw University of Technology, Institute of Aeronautics and Applied Mechanics, Nowowiejska 24, 00-661 Warsaw, Poland. Email: mpocwie@meil.pw.edu.pl,*

[2]*Warsaw University of Technology, Faculty of Architecture, Koszykowa 55, 00-659 Warsaw, Poland. Email: katarzyna.zielonko-jung@arch.pw.edu.pl*

Many scientific papers apply to computer simulations related to wind engineering, comparison of experimental data results and proper modelling of the boundary layer [1–15]. All this led to the formation of a new domain – the Computational Wind Engineering (CWE). In his paper [16], Blocken summarizes the achievements in this area over the last 50 years and predicts further developments. His article contains an accurate review of the literature and trends in the field of mechanics.

This paper considers one of the issue connected with CWE – wind comfort in a housing estate, which is widely described in [17, 18]. City authorities, investors and especially all of us who live in the urban space have noticed problems, which are side effects of the wind. In some cases, the need for the aerodynamic expertise of the expanded or new buildings is required by law. Such situation arises when they are located in the aeration tunnels which provide ventilation in the city [19, 20]. Some investors order special tests in order to improve the attractiveness of the offered estates. The purposes of conducting such an analysis are: minimization of the stagnation zones (which gather pollution and odours); reduction of the impact of onerous gusts of wind which threaten human health and life; proper placement of windows, doors, gates and ventilation outflows; prediction of the acoustic effects caused by components' vibration related to the streams of airflow, through various cracks.

Despite the significant development of CFD and many scientific papers related to the airflow around the buildings, in the article [21], Blocken points out the importance of the experimental validation of the model. It is particularly significant during the study of complex architecture systems, where the problems connected with modelling of turbulence in the boundary layer are most noticeable. Many of the errors contained in RANS models, such as overestimation of the separation zone length behind the obstruction (for example the building) and underestimation of the speed in the back, do not occur while using the LES model (Large Eddy Simulation), which is shown in the article [2]. However, the numerical process is still too expensive to study a larger group of buildings, because usually we do not have enough computing power and the researchers only predict its development [16]. That is why authors decided to study not only the numerical part, but also do a comprehensive research of the complex architectural quarter in the wind tunnel. The analysis, which includes measurement of pressure, techniques using sand erosion and oil visualization, has been performed.

The main aims of this paper are: accurate research on urban quarter; performance of numerical simulations which use the turbulence k-ε realizable model [2, 16, 22] and the seven-equation RSM model (Reynolds Stress Model) [11, 23, 24]; comprehensive comparison of numerical and experimental results for different layout configurations and turbulence models, as well as discussion over its usefulness in modelling flow around buildings.

2. Model description

2.1. Actual geometry

The subject of the study is an urban quarter in a hypothetical setting. This is an example of a typical situation when the C-shaped building is surrounded by compact buildings. The model includes two basic types of urban systems: streets and a courtyard inside the square. The dimensions and proportions of the building chosen comply with building regulations regarding issues like the right to access to daylight, mutual obscurity and fire regulations. They emulate typical conditions of densely populated districts of large cities. The C-shaped building with an opening was studied (Fig. 1). The system dimensions are shown in the sketch. All buildings are 18 m high.

For the purposes of testing in the wind tunnel, the size of the buildings was scaled down, using 1: 400 scale. The scaled dimensions were used for the numerical simulation.
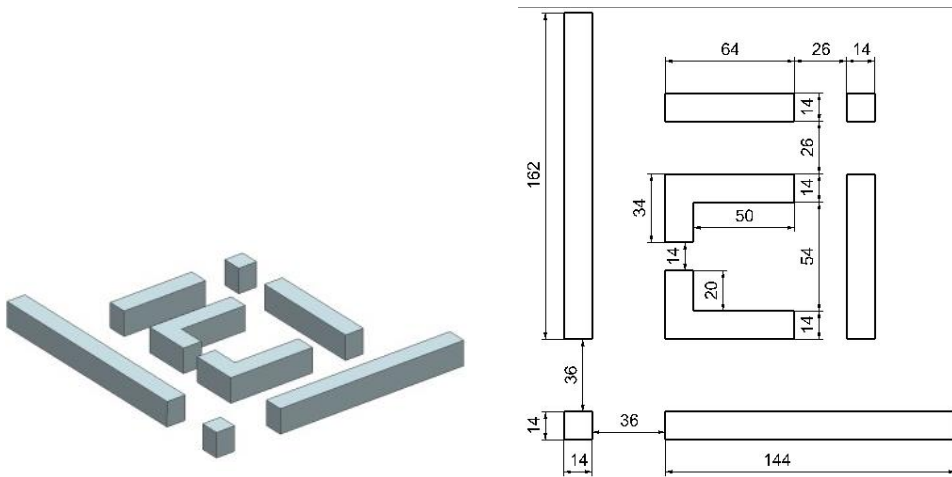

Fig. 1. Shape of the analyzed urban quarter and the actual dimensions of the buildings [m]

3. Experimental research

Experiments were conducted in a wind tunnel with a 1-metre square cross-section. It is necessary to generate an appropriate boundary layer while carrying out measurements of an airflow around buildings in the standard tunnel. In that case, a set of adequate spires and obstacles was used to achieve an expected profile of velocity and the desired intensity of turbulence. This group of obstacles was placed at the bottom of the tunnel in the formation section, in the area in front of

the model (Fig. 2). The method used for distribution of these elements in order to make them disrupt the flow of the wind tunnel suitably was adopted according to the study [20] and [25].

Fig. 2. Elements shaping the profile of velocity

The velocity and intensity profiles were measured by thermoanemometer in several places (about 90) located along the tunnel height. When the probe was closer to the base of the tunnel the distance between measurement points was less (the smallest distance was equal 0.05 mm). The average speed u_n and speed fluctuation u'_n (standard deviation of the speed) were measured directly along the direction of the flow.

Five measurements were made for each point, and each measurement was obtained by averaging the readings of the probe for a period of 3 seconds. The reading accuracy was about 0.2 m/s. Data from experimental studies were interpolated and then used in numerical simulation. The dimensionless velocity and intensity profiles are shown in Fig. 3.
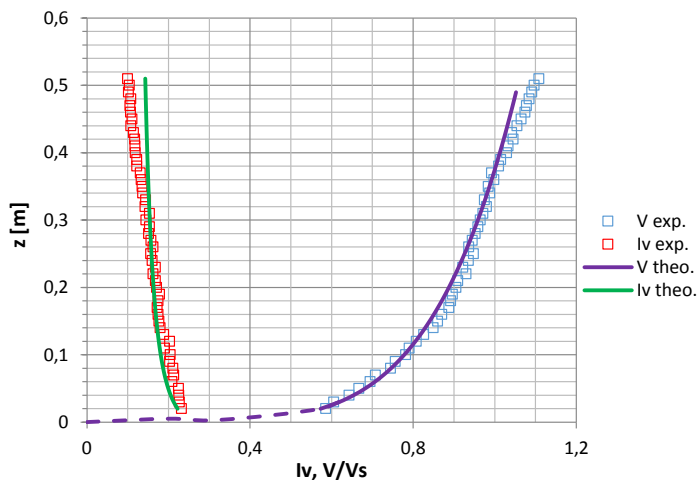

Fig. 3. The dimensionless velocity and turbulence intensity profiles (solid lines present theoretical results and squares – measurement results)

The theoretical velocity profile was obtained using the formula

$$V = V_s \left(\frac{z}{z_s} \right)^{\alpha} \tag{1}$$

where V_s is the velocity at reference height z_s (in our case $z_s = 0.375$ mm which corresponds to 10 m in full scale) and α is the power – law exponent determined by the terrain category (in our case $\alpha = 0.19$). The profile of turbulence intensity was calculated from equation

$$I(z) = \frac{1}{\ln \left(\frac{z}{z_0} \right)} \tag{2}$$

where z_0 is the boundary layer height determined by terrain category (in our case $z_0 = 0.5$ mm).

Measurement methods used for analysing an airflow around buildings can be divided into two groups: point and planar. The first of them provides a piece of numerical information about an arbitrary physical quantity, e.g. velocity or pressure. This method is limited to the finite amount of points. The other one provides continuous qualitative information on a certain value in a certain area [21]. One of the point methods was used during the research – that is measuring the pressure with a group of water gauges – and two planar methods – namely, oil visualization and sand erosion were applied. The former method shows the direction of the flow, while the second one informs about velocity changes that result from the presence of obstacles on its way and are compared to an undisturbed flow. The important parameter describing those changes is the speed gain factor α, hereafter referred to as coefficient of wind amplification. (Article [21] explains explicitly how to exactly determine this coefficient). The relation

$$\alpha_n = \frac{U_{GB}}{U_{G,n}} \tag{3}$$

defines this coefficient, where U_{GB} denotes the ground-level wind speed that is influenced by the building and for which sand erosion occurs, and $U_{G,n}$ denotes the ground-level wind speed that is not influenced by the building. Using the following equalities

$$\frac{U_{W,1}}{U_{G,1}} = \frac{U_{W,2}}{U_{G,2}} = \cdots = \frac{U_{WB}}{U_{GB}} \tag{4}$$

this coefficient may also be written in the form $\alpha_n = \dfrac{U_{WB}}{U_{W,n}}$ where U_{WB} denote the wind tunnel operating speed for which sand is blown away from the floor (in this case the floor is without building models). In the second step, the building models are placed on the floor, which is sprinkled with fine layer of sand. Wind tunnel speed is increased in steps ($U_{W,1}, U_{W,2} \ldots U_{W,n} \ldots$) and the sand erosion that

occurs at each case is allowed to reach a steady state. In the area where $\alpha > 1$ the flow accelerates, e.g., because of buildings. Conversely, for $\alpha < 1$ the flow slows down.

Measurement of the pressure was carried out primarily in order to compare the numerical model with the experimental one. The pressure was measured in defined points between buildings with the use of water gauges' battery connected to the model using rubber tubing. The readings were taken automatically by the system connected to the computer. The accuracy was ±1 Pa.
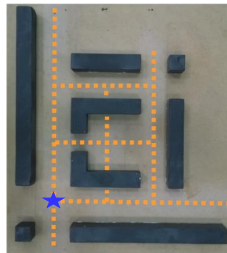

Fig. 4. Distribution of pressure measurement points

In Fig. 4, the position of pressure measurement points in the channels between the buildings and in the central square is shown. 104 measurement points were created, while the distance between every two of them was limited to 20 mm. Path points ran in the middle of the distance between buildings. The point marked with an asterisk is at a distance of 45 mm both from the buildings located horizontally (bottom of the Fig. 4) and vertically (left side of the Fig. 4). The pressure measurement was performed at least 8 times at each point, so that the arithmetic mean could be determined. The standard deviation of the pressure measurements for individual points is enclosed within the range: $\sigma \in (0; 0.8)$ Pa. Examples of the results of pressure measurements at points (distributed along the line indicated in Fig. 4) and with marked 95% confidence intervals are shown in Fig. 5. Errors were estimated according to the methods described in [26].
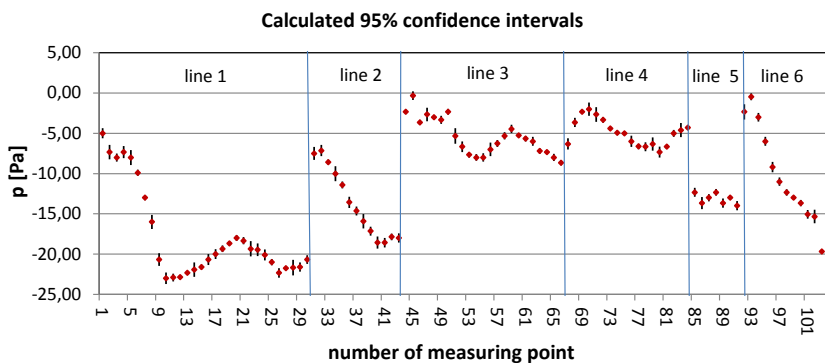

Fig. 5. The pressure measurements at points with 95% confidence

4. Calculation model

4.1. Geometry of numerical domain

The computational domain is presented in Fig. 6. The height of the domain is 0.625 m. It is suggested [15] that this dimension should be at least 5 times higher than the highest building h_b (in this case h_b = 0.045 m). For urban areas with multiple buildings, the lateral boundaries of the computational domain can be placed about 5 height of the tallest building to that part of the built area which surrounds the region of interest [5, 27]. In the case under consideration, the size of the domain on the lateral direction is equal to 1.25 m and satisfies the condition described above, but it is larger than the size of the wind tunnel in that direction. This can cause some change in the flow and have a little effect on the results. The other dimensions meet the criteria presented in literature [5, 15, 21, 27].
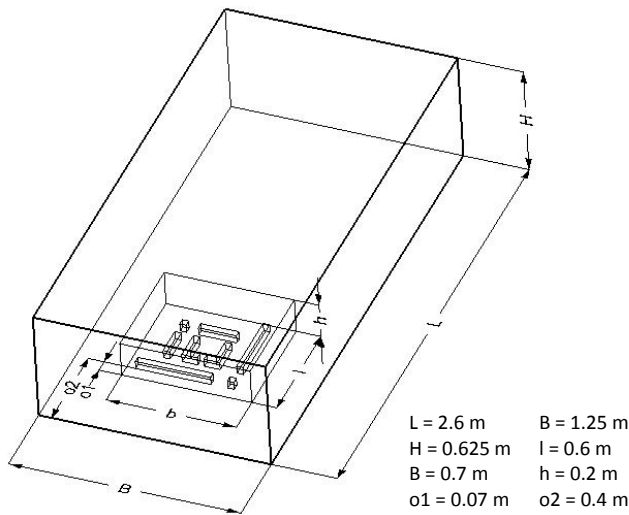

L = 2.6 m	B = 1.25 m
H = 0.625 m	l = 0.6 m
B = 0.7 m	h = 0.2 m
o1 = 0.07 m	o2 = 0.4 m

Fig. 6. Model of numerical domain

According to the tests conducted in [25], a structured grid was used. There were 0.005 m = $1/9h_b$ long cells in the high-density zone (space size $b \times l$, Fig 7). It was verified that this mesh size for the test speed allows for obtaining the dimensionless ratio of the wall distance $y_+ \in (15; 60)$ [15, 22, 28]. This parameter is significant in the boundary layer theory. Near the walls, volume of the cells should be of such a size that non-dimensional wall distance from their centroids satisfies the condition $15 < y_+ <\sim 300$. However, a more restricted rule, $y_+ \in (30, 60)$, is recommended. Outside this boundary, the finite volumes grow with the coefficient of 1.2 in each direction, as it is proposed in [27]. Fig. 7. presents the distribution of the finite volumes mesh. The whole mesh consists of roughly 2.5 million elements.
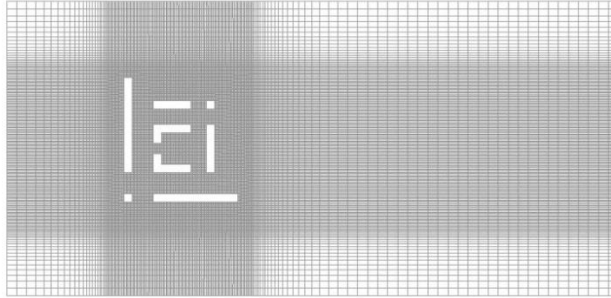
Fig. 7. Close-up of the computational grid, cross-section in a plane XY

The distance between the inlet boundary and elements disturbing airflow must be large enough. Otherwise, the inflow boundary conditions can be strongly in-homogeneous. On the other hand, long distance can prove to change the inflow parameters close to buildings, which results in a mismatch between computational and experimental conditions of the airflow. This distance was set to be $11h_b$ as it is mentioned in [11].

The model was rotated about 90 degrees for the second wind direction and then a new grid was created in a similar manner to the previous case.

The velocity, turbulent kinetic energy and dissipation rate inlet profiles were used (Fig. 8). They were prepared with velocity magnitude and velocity fluctuation measured and interpolated. Evolution of the velocity profile in the area before buildings was observed as [10] suggests. Results of experiment and of numerical simulation coincided well.
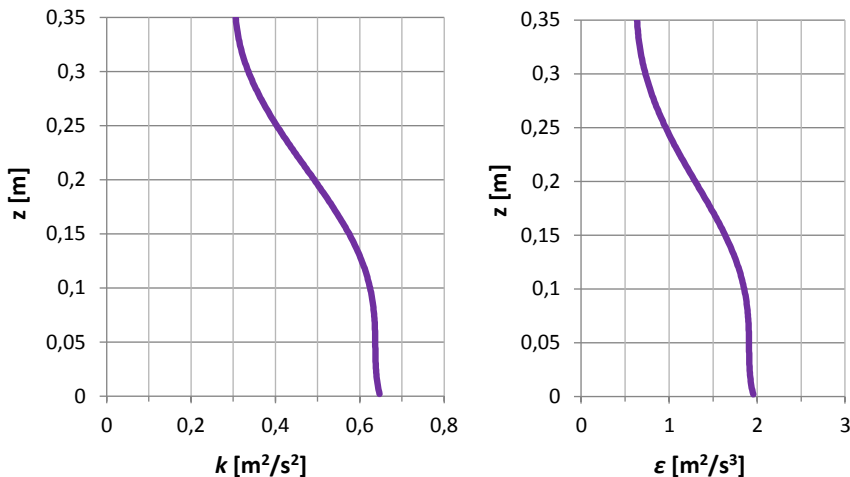

Fig. 8. Profiles of the turbulent kinetic energy and dissipation rate used for calculation after interpolation

The turbulent kinetic energy was obtained from:

$$k = \frac{1}{2}(u_i^2) = \frac{3}{2}u_n'^2 \tag{5}$$

where u_n' is standard deviation of the speed. The dissipation rate is given by

$$\varepsilon = C_\mu^{3/4} \frac{k^{3/2}}{\kappa z} \tag{6}$$

where z is the distance between the definition point and wall, C_μ is a model constant (= 0.09) and κ is the Kármán constant (= 0.4).

Fluids pressure and velocity at the outflow of the computational area are usually unknown. In models of flow around bodies, there should be an appropriate distance between this boundary and the last body (here approximately $30h_b$), just to avoid the impact of wake effects on airflow.

4.2. Numerical calculation

The simulation was performed using the FLUENT 15.0. software. Wall condition was given on surfaces of the buildings and the computational domain boundaries. The condition type no slip was applied on surfaces of the buildings and on the lower plane of computational domain while specified shear condition was assumed on the top surface and site walls (all components of shear stress were equal 0).

The incompressible model of flow with a constant density and kinematic viscosity was applied to calculations. According to the recommendations contained in [5, 28], the following settings were adopted. Steady air flow was applied, which is a common method for modelling airflow around buildings. In practice, URANS model (Unsteady RANS) is rarely used because it is time-consuming and because the results are worse than those obtained from equally time-consuming LES model [3]). The pressure based solver of double precision and the standard method (which is, by default, recommended in Fluent [30]) to interpolate the pressure was used.

SIMPLE algorithm, which is based on the segregated method, was applied to calculations. Two models of turbulence were adopted:
  a. k-ε realizable model (**RKE**)
     This is a modification of one of the most popular turbulence models in the RANS group (average Reynolds time was used). k-ε models are based on Bousinessqu hypothesis, which assumes that the Reynolds stresses are proportional to the speed of deformation. According to the standard k-ε model, the way the equations define the turbulent dissipation rate and the turbulence viscosity are the most significant differences. The exact description of both methods can be easily found in the literature, e.g. [8, 16, 17, 22, 25, 28].

   b. Reynolds Stress Model **RSM**
      This is the most elaborate turbulence model that FLUENT provides. Abandoning the isotropic eddy-viscosity hypothesis, the RSM closes the Reynolds-averaged Navier-Stokes equations by solving transport equations for the Reynolds stresses (6 components), together with an equation for the dissipation rate. This means that seven additional transport equations must be solved in 3D, what makes this model 2 times more numerically expensive than the 2-equation RKE model. This method is fully described in [24, 28].

RSM is still being developed and convergence problems might appear while using it. On the other hand, it models a greater variety of phenomena in a greater detail and can be more suitable for complex problems, which contain secondary flow, large zones of detachment, highly swirling flows. According to that fact, as well as to having large enough computing power, the authors decided to test this model of turbulence. Additionally, results included in [11] showed that it is possible to get a better convergence with the experiment than using a k-ε realizable model. It needs to be highlighted that tests presented in this article were provided for relatively simple geometry.

In general, high Reynolds number flows are simulated realistically by turbulence models, as viscous stresses (related to the molecular viscosity) are small in comparison to Reynolds stresses. Close to the walls, Reynolds number decreases, while viscous stresses increase. Thus, other way of turbulence simulation must be introduced. The standard wall function was chosen according to the rules found in [22, 28, 29]. This model lets cells close to buildings be larger, which reduces calculation time.

In this case, a linear pressure–strain model without wall reflection effects was used to calculation. The Reynolds stress component was obtained from the turbulent kinetic energy k. Isotropy of the turbulence was assumed in the same way as in [30].

Second-order upwind method was selected for discretization of momentum and other transport equations for RKE and RSM models. The convergence of both solutions (RKE and RSM) was monitored by the observation of the residuals values. The continuity equation for which achieved the convergence $4 \cdot 10^{-4}$ was decisive for the solution. Residuals values for velocity oscillated around 10^{-5}.

5. Comparison of pressure and velocity for two models of turbulence

Velocity, streamlines and pressure measured in experiments and computed in simulations are compared in this chapter. In the case of velocity and streamlines, west wind for the geometry described in section 2 is analysed, while the comparison of pressure is presented for west and north direction of the wind. These two directions of wind occur most frequently in Poland.

5.1. Comparison of the images of oil visualisation and sand erosion with velocity maps obtained from calculations

Contour maps (Fig. 9a,b) present coefficient of the wind amplification for two turbulence models – RKE, RSM and were measured using sand erosion (Fig. 10b). The value of 5.7 m/s was taken as the speed at the ground for air flow without a building. This measurement result was obtained at the height of 2.5 mm and was made during the test of the velocity profile development. Additionally, there is a map of oil visualisation, in which vortex structures and direction of the flow (Fig. 10a) are represented.

Experimental methods generate results similar in nature to the numerical simulations. Both of the turbulence models correctly represent small recirculation
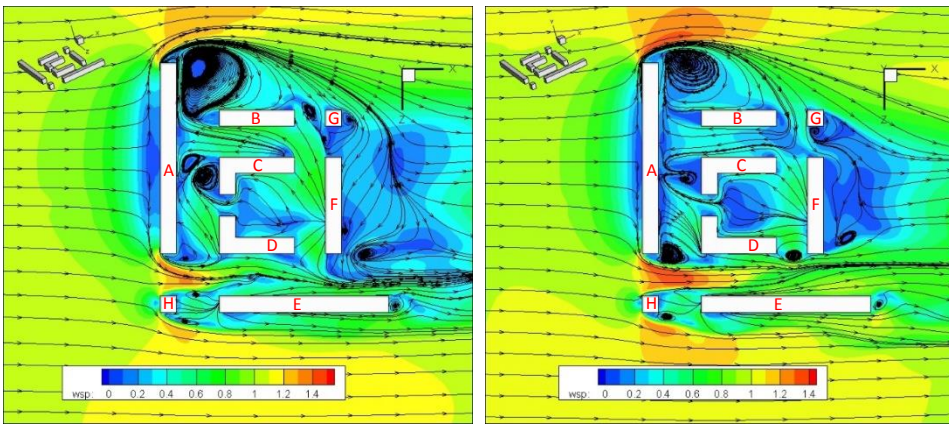

Fig. 9. Contour map of wind amplification factor with streamlines using RKE (a) and RSM (b) turbulence model
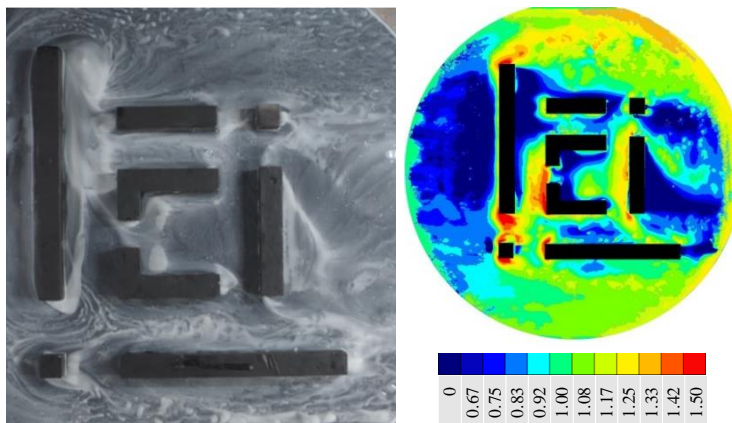

Fig. 10. Oil visualization (a) vs. sand erosion (b), west wind

eddies behind buildings E, G, and H. On the other hand, the bigger ones, followed by building A, cover too large an area. This fact may be due to the problems of k-ε models that have a tendency to overestimate kinetic energy of turbulence [22], which results in differences of size and location of vortexes compared to experiments. However, using RSM did not improve this significantly. The composition of vortices and streamlines are not the same behind the analysed quarter for two turbulence models. It is difficult to judge which one is more appropriate, as this is a strongly turbulised region of a complex flow. A wide area of stagnation is the only thing which can be noticed looking at this region on oil visualisation and sand erosion.

Both models simulate a correct direction of the flow, including reversed flow between buildings B-C, C-D and in the central part of the quarter. As it was mentioned in [21], the amplification factor of the wind should not be compared quantitatively between buildings. Numerical simulation has a tendency to understate values and reduce the number of areas of intensified flow. The effect of wind nozzle between buildings A and H is modelled properly using both models of turbulence. On the other hand, they do not show a zone of accelerated flow in front of building D. The range of the amplification factor is similar both in the case of numerical simulation and experiment and is equals about 1.4.

5.2. Comparison of the pressure

The following maps (Fig. 11 – west-side airflow and Fig. 13 – north-side airflow) present pressure distribution in the analysed urban setting. The lines symbolise places, where the measurements in the wind tunnel were conducted while arrows show the end of each measuring line.
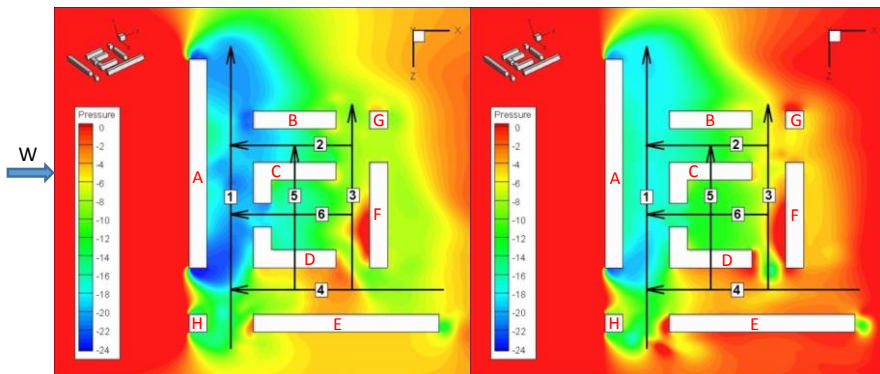

Fig. 11. Contour map of the pressure, west wind, RKE (a) vs. RSM (b) model

At the beginning of the analysis of pressure coefficient diagrams (Fig. 12), it should be noticed that both models reproduce experimental results in a highly accurate manner. There are some areas where the RKE model works better (e.g.
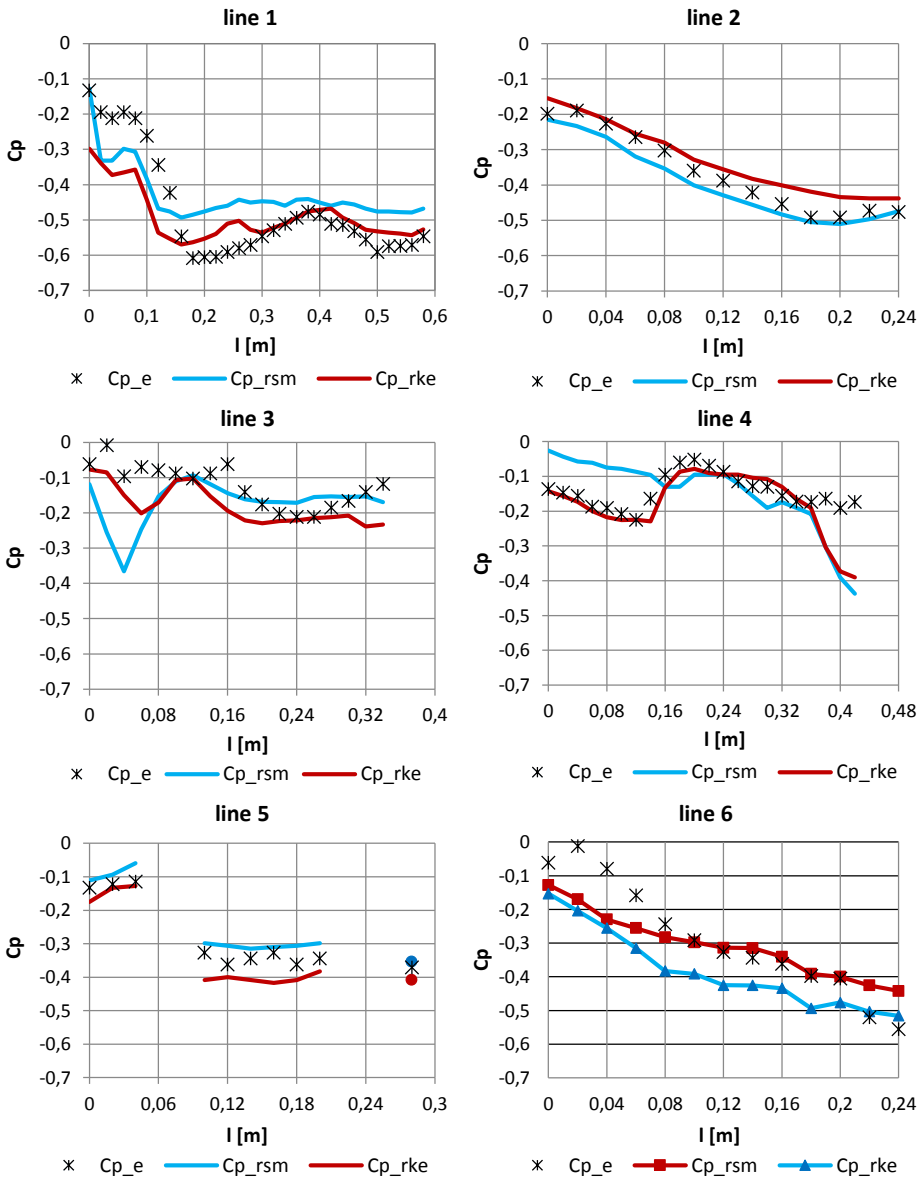
Fig. 12. Diagrams of the pressure coefficient along the paths (lines 1- 6), west wind

second part of line 1, line 4). On the other hand, the RSM model seems to be more precise at line 5 or the centre of line 6. Pressure coefficients obtained using RSM model are slightly higher than the RKE model's ones. The most significant differences between experiments and numerical simulation appear in the area of strong vortices and air turbulence. It is visible at the borders of line 4. Pressure

coefficient values are lower by 0.1-0.2 compare to the ones measured here. There is a recirculation vortex at the place just behind the building A. As it was explained in the previous chapter, turbulence models show a tendency to overestimate the level of the kinetic energy of turbulence. This leads to an increase in the area of the vortex, where the pressure is reduced. The beginning of line 1 is another discrepancy in results. There is a reflection of the wind stream which connects to other flows around other buildings.

As it was mentioned above, Fig. 13 shows a distribution of pressure for north-side wind inflow and the test lines placed on the map.
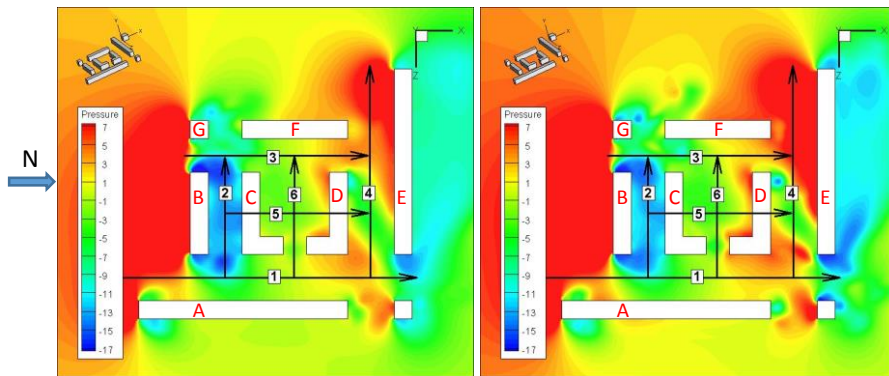

Fig. 13. Contour map of the pressure, north wind, RKE (a) vs. RSM (b) model

The values of the pressure coefficient derived from numerical simulation match the ones measured (Fig. 14). In contrast to the previous configuration, the calculated pressure coefficient is mainly overestimated now. Again, there are no proof that using RSM makes the results more accurate.

6. Summary and conclusions

The analysis describes a complex air flow around a group of buildings. Using a variety of methods of experimental fluid mechanics, such as pressure measurement, sand erosion and oil visualization, an urban quarter with two modifications was examined. The latest trends in the field of CWE presented for example in articles [10, 12, 16], were used while creating numerical simulations. Not only was the airflow around buildings described, which is helpful from architects' point of view, but also the usefulness of the RSM model of turbulence was tested. The experimental results obtained, supplemented by numerical calculations gave a full picture of the phenomena occurring in the tested configurations of buildings and allowed for exact interpretation. Summing up all data, the following conclusions can be drawn:

- Turbulence models (k-ε *realizable* and *Reynolds Stress Model*), which are used for studying the phenomena of the air flow around buildings describe
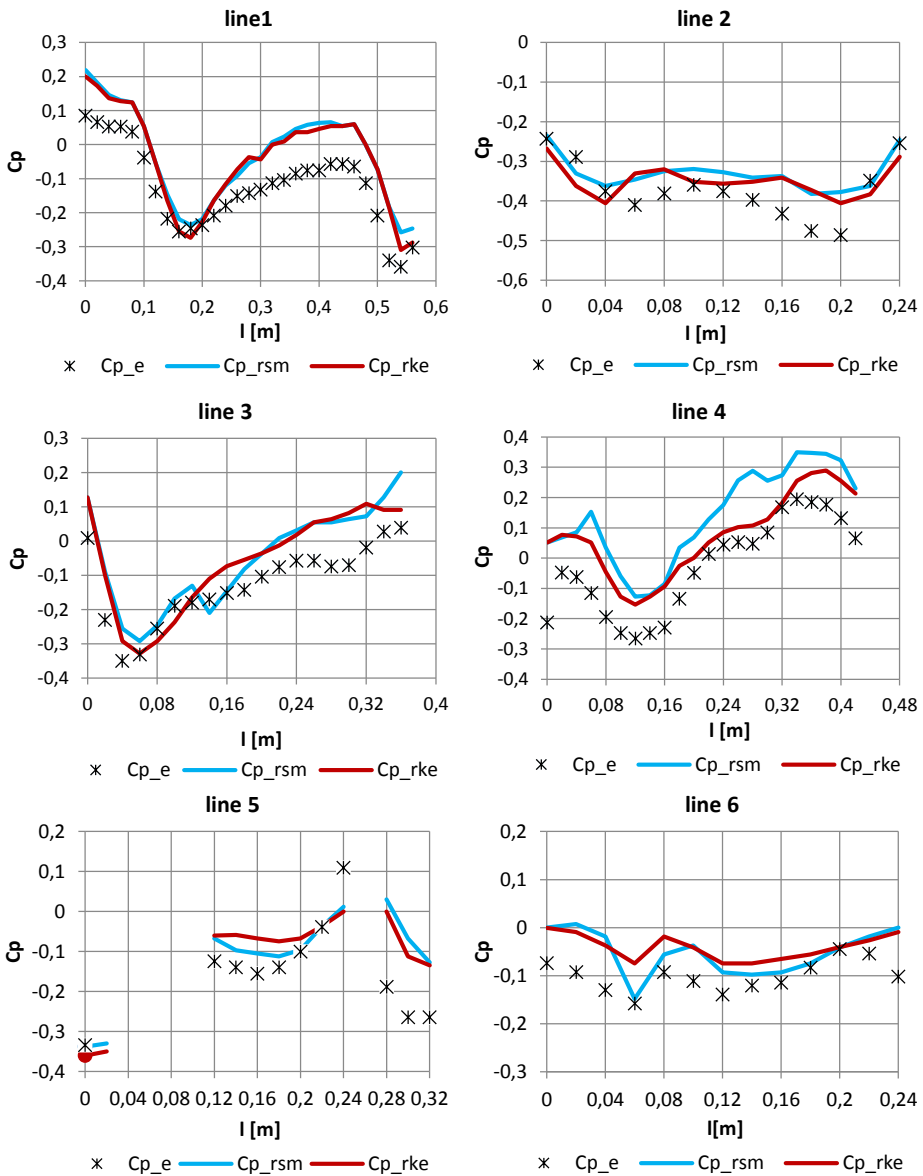
Fig. 14. Diagrams of the pressure coefficient along the paths (lines 1-6), north wind

them properly but are not their accurate representation. In general, the results correspond to the experimental data, while little differences will be getting smaller with the further development of the CFD technique.

- Two turbulence models were analysed. There was no reason for using a more complex method, namely the seven equation model RSM (Reynolds Stress

Model). The time needed for calculation using RSM model was almost twice as long as that required for the popular model k-ε realizable and the results were not more accurate. In [11], it was mentioned that RSM gives more accurate results when analysing simple airflow around the block. For a more complicated geometry, the results were not improved by using RMS model.

- The bigger differences in the values of pressure coefficient obtained were noticeable in the areas of strong vortex. This exposes current problems of turbulence modelling, as RANS models seem to work worse in such cases.

The study also allowed for some observations of the selection of the optimal configuration of settlement.

- In the analysed situation, the introduction of an opening brings positive results. It does not lead to a significant acceleration of the air flow in the vicinity, but significantly reduces the size of areas of stagnation in the court-yard, which in turn improves local ventilation.
- The differences for studied configurations (the C-shaped building with open-ing, which is presented in this article and the C-shaped building as a solid block discussed in [26]) are not big and the changes occur only in the lo-cal area. The final choice of an appropriate method should be supported by economic factors, land development conditions, aesthetics, functionality etc.

References

[1] R. Yoshie, A. Mochida, Y. Tominaga, H. Kataoka, K. Harimoto, T. Nozu, and T. Shirasawa. Cooperative project for CFD prediction of pedestrian wind environment in the Architectural Institute of Japan. *Journal of Wind Engineering and Industrial Aerodynamics*, 95(9):1551–1578, 2007. doi: 10.1016/j.jweia.2007.02.023.

[2] A. Mochida and I.Y.F. Lun. Prediction of wind environment and thermal comfort at pedestrian level in urban area. *Journal of Wind Engineering and Industrial Aerodynamics*, 96(10):1498–1527, 2008. doi: 10.1016/j.jweia.2008.02.033.

[3] B. Blocken, T. Stathopoulos, J. Carmeliet, and J.L.M. Hensen. Application of computational fluid dynamics in building performance simulation for the outdoor environment: an overview. *Journal of Building Performance Simulation*, 4(2):157–184, 2011. doi: 10.1080/19401493.2010.513740.

[4] S.E. Kim and F. Boysan. Application of CFD to environmental flows. *Journal of Wind Engineering and Industrial Aerodynamics*, 81(1):145–158, 1999. doi: 10.1016/S0167-6105(99)00013-6.

[5] J. Franke, A. Hellsten, K.H. Schlunzen, and B. Carissimo. Best practice guideline for CFD simulation of flows in the urban environment: a summary. University of Hamburg, Hamburg, 2007.

[6] J. Franke, A. Hellsten, K.H. Schlunzen, and B. Carissimo. The cost 732 best practice guideline for cfd simulation of flows in the urban environment: a summary. *International Journal of Environment and Pollution*, 44(1-4):419–427, 2011. doi: 10.1504/IJEP.2011.038443.

[7] S. Murakami, A. Mochida, and Y. Hayashi. Examining the k-ε model by means of a wind tunnel test and large-eddy simulation of the turbulence structure around a cube. *Journal of Wind Engineering and Industrial Aerodynamics*, 35:87–100, 1990. doi: 10.1016/0167-6105(90)90211-T.

[8] D.A. Köse and E. Dick. Prediction of the pressure distribution on a cubical building with implicit LES. *Journal of Wind Engineering and Industrial Aerodynamics*, 98(10):628–649, 2010. doi: 10.1016/j.jweia.2010.06.004.

[9] P.J. Richards and S.E. Norris. Appropriate boundary conditions for computational wind engineering models revisited. *Journal of Wind Engineering and Industrial Aerodynamics*, 99(4):257–266, 2011. doi: 10.1016/j.jweia.2010.12.008.

[10] D.A. Köse, D. Fauconnier, and E. Dick. ILES of flow over low-rise buildings: Influence of inflow conditions on the quality of the mean pressure distribution prediction. *Journal of Wind Engineering and Industrial Aerodynamics*, 99(10):1056–1068, 2011. doi: 10.1016/j.jweia.2011.07.008.

[11] S. Reiter. Validation process for CFD simulations of wind around buildings. In *Proceedings of the European Built Environment CAE Conference*, pages 1–18, London, June 2008.

[12] A. Kovar-Panskus, P. Louka, J.F. Sini, E. Savory, M. Czech, A. Abdelqari, P.G. Mestayer, and N. Toy. Influence of geometry on the mean flow within urban street canyons – a comparison of wind tunnel experiments and numerical simulations. *Water, Air, and Soil Pollution: Focus*, 2(5):365–380, 2002. doi: 10.1023/A:1021308022939.

[13] B. Blocken and J. Persoon. Pedestrian wind comfort around a large football stadium in an urban environment: CFD simulation, validation and application of the new Dutch wind nuisance standard. *Journal of Wind Engineering and Industrial Aerodynamics*, 97(5):255–270, 2009. doi: 10.1016/j.jweia.2009.06.007.

[14] M. Sakr Fadl and J. Karadelis. CFD simulations for wind comfort and safety in urban area: A case study of Coventry University central campus. *International Journal of Architecture, Engineering and Construction*, 2(2):131–143, 2013. doi: 10.7492/IJAEC.2013.013.

[15] B. Blocken, T. Stathopoulos, and J. Carmeliet. CFD simulation of the atmospheric boundary layer: wall function problems. *Atmospheric Environment*, 41(2):238–252, 2007. doi: 10.1016/j.atmosenv.2006.08.019.

[16] B. Blocken. 50 years of Computational Wind Engineering: past, present and future. *Journal of Wind Engineering and Industrial Aerodynamics*, 129:69–102, 2014. doi: 10.1016/j.jweia.2014.03.008.

[17] A. Flaga. *Wind Engineering*. Arkady, Warsaw, Poland, 2008. (in Polish).

[18] K. Klemm. A complex assessment of microclimate conditions found in widely spaced and dense urban structures. KILiW, Polish Academy of Sciences, 2011. (in Polish).

[19] K. Daniels. *The Technology of Ecological Building*. Birkhäuser, Basel-Boston-Berlin, 1997.

[20] R. Jóźwiak et al. An analysis of a potential influence on airing and wind conditions of the area surrounding an urban layout planned to be built at a lot situated in warsaw, powązkowska street 23/1. Warsaw University of Technology, 2013. internal, not published materials of Institute of Aeronautics and Applied Mechanics, (in Polish).

[21] B. Blocken and J. Carmeliet. Pedestrian wind environment around buildings: Literature review and practical examples. *Journal of Thermal Envelope and Building Science*, 28(2):107–159, 2004. doi: 10.1177/1097196304044396.

[22] E. Błazik-Borowa. *Difficulties arising from the use of k-ε turbulence model for the purpose of determining the airflow around buildings*. Lublin University of Technology Publisher, 2008. (in Polish).

[23] S. Murakami. Overview of turbulence models applied in CWE–1997. *Journal of Wind Engineering and Industrial Aerodynamics*, 74:1–24, 1998. doi: 10.1016/S0167-6105(98)00004-X.

[24] K. Hanjalic and B.E. Launder. A Reynolds stress model of turbulence and its application to thin shear flows. *J. Fluid Mech*, 52(4):609–638, 1972. doi: 10.1017/S002211207200268X.

[25] K. Gumowski, O. Olszewski, M. Poćwierz, and K. Zielonko-Jung. Comparative analysis of numerical and experimental studies of the airflow around the sample of urban development. *Bulletin of the Polish Academy of Sciences Technical Sciences*, 63(3):729–737, 2015. doi: 10.1515/bpasts-2015-0084.

[26] J.R. Taylor. *Introduction to Error Analysis*. University Science Books, 2nd edition, 1996.

[27] Y. Tominaga, A. Mochida, R. Yoshie, H. Kataoka, T. Nozu, M. Yoshikawa, and T. Shirasawa. AIJ guidelines for practical applications of CFD to pedestrian wind environment around buildings. *Journal of wind engineering and industrial aerodynamics*, 96(10):1749–1761, 2008. doi: 10.1016/j.jweia.2008.02.058.

[28] *Ansys Fluent Theory Guide, version 14.0*. Canonsburg, 2011.

[29] *Ansys Fluent User's Guide, version 14.0*. Canonsburg, 2011.

[30] H. Montazeri and B. Blocken. CFD simulation of wind-induced pressure coefficients on buildings with and without balconies: validation and sensitivity analysis. *Building and Environment*, 60:137–149, 2013. 10.1016/j.buildenv.2012.11.012.